

Tissue–Blood Exchange of Extravascular Longitudinal Magnetization with Account of Intracompartmental Diffusion

José R. Solera Ureña,^{1*} Salvador Olmos,¹ and Valerij G. Kiselev²

The joint effect of both extravascular water diffusion and transcapillary water exchange on the longitudinal magnetisation is evaluated theoretically for tissues with sparse capillary networks (e.g., the brain and myocardium). The spatio-temporal profile of the extravascular longitudinal magnetisation is calculated for the limiting case of a high blood concentration of paramagnetic tracer resulting in negligible intravascular magnetisation, hence in a net flux of magnetisation from the extravascular tissue to its contained blood. A related parameter, termed the effective extravascular depolarised volume, is derived that quantifies the ensuing attenuation of the NMR signal and affords a taxonomy of exchange regimes. It is found that the spatio-temporal pattern of magnetisation decay may deviate strongly from that predicted by chemical exchange models when the rate of transcapillary exchange is limited by slow diffusive transport in the extravascular tissue but reproduces known results in the case of fast extravascular diffusion. Magn Reson Med 000:000–000, 2011. © 2011 Wiley-Liss, Inc.

Key words: tissue–blood exchange; intracompartmental diffusion; permeability; extravascular depolarised volume; Green's function; paramagnetic contrast agents

INTRODUCTION

Water exchange between physiologic compartments is essential to tissue function and can be probed by MRI using paramagnetic contrast agents. Compartmental water exchange must be accounted for when quantifying the effect of MRI tracers (1). The purpose of this work is to evaluate theoretically the flux of extravascular longitudinal magnetisation between a tissue and its contained blood, with account of spin diffusion in the extravascular space. Specifically, we consider the limiting case of negligibly low intravascular magnetisation produced by a high concentration of paramagnetic blood-pool tracer, resulting in a net flux of extravascular magnetisation across the capillary wall and into the blood pool. The term

tissue–blood exchange shall be used in the sequel with this precise meaning. We begin by reviewing previous work on the effect of paramagnetic blood-pool tracers and extravascular water proton diffusion on the NMR signal.

Exogenous paramagnetic contrast agents (e.g., gadolinium chelates and macromolecules) affect water magnetisation by increasing the local relaxation rate, as well as through indirect, long-ranged susceptibility effects (1) that reach virtually all tissue protons; as a result, complex magnetic interactions ensue at the mesoscopic scale (ca. 1 – 100 μm) of cells and microvessels.

Relaxation effects: Blood-pool tracers increase the local transverse and longitudinal relaxation rates of plasma (as well as its magnetic susceptibility) through electron-nuclear dipole interactions experienced by water molecules diffusing near the tracer particles (2–4). Such relaxation effects then propagate to adjacent physiologic compartments through water proton exchange (5); whilst plasma–erythrocyte water exchange is considered to be fast (in the range of milliseconds) (1), tissue–blood exchange can, at a given time, occur in one of several regimes, as discussed in this work. Bauer and Schulten (5) used the Bloch-Torrey equation (6) and the mean relaxation time approximation (7) to determine the mean relaxation time in whole tissue as a function of capillary density, capillary water permeability and compartmental diffusivity. The compartmental mean relaxation times were then incorporated into a pharmacokinetic model that accounted for tissue perfusion and transcapillary water exchange (8). Based on this model, a number of studies have demonstrated the feasibility of T_1 -based measurements for the extraction of transcapillary water exchange rates (9,10), perfusion rate in in vivo animal models (11,12), and intracapillary blood volume using blood-pool tracers (10,13).

Susceptibility effects: Magnetic susceptibility differences between blood and extravascular tissue induce long-ranged magnetic field gradients, leading to a several-fold increase in the effective transverse relaxivity of the tracer in tissue relative to that of whole blood (14,15) and hence to strong signal attenuation. The theory of susceptibility-induced NMR signal dephasing, cf. Refs. 16–19 and references therein, is not considered further in this study, which is mainly concerned with the longitudinal magnetisation.

In chemical exchange theory, the Bloch equations are augmented with first-order exchange terms (20,21); intracompartmental diffusion is assumed to be much faster than both magnetic relaxation and compartmental exchange (“well-mixed” assumption). Formulae for T_1 and T_2 can be found in, e.g., Refs. 21–23, with discussion of important special cases. For a given exchanging

¹Biomedical Engineering Division, Aragón Institute of Engineering Research, Universidad de Zaragoza, Zaragoza, Spain

²Department of Radiology, Medical Physics, University Medical Center Freiburg, Freiburg, Germany

Grant sponsor: Ministry for Science and Innovation, Spain; Grant numbers: TEC2006-13966-C03-02, TEC2009-14587-C03-01; Grant sponsor: CONAID-CAI (Aragón, Spain); Grant number: CM 3/09

*Correspondence to: José Rufino Solera Ureña, B.Eng., Depto. Ingeniería Electrónica y Comunicaciones, Edificio Ada Byron, C/ María de Luna, 1, 50018 Zaragoza, Spain. E-mail: solera@unizar.es

Received 14 May 2010; revised 11 February 2011; accepted 18 February 2011.

DOI 10.1002/mrm.22919

Published online in Wiley Online Library (wileyonlinelibrary.com).

species, a compartmental system is said to be in slow chemical exchange if the difference between the water relaxation rates in the exchanging compartments [i.e., the MR relaxographic shutter speed (24)] greatly exceeds the first-order exchange rates involved (9,24) and is said to be in fast exchange in the opposite case, with a range of intermediate cases. Knowledge of the exchange regime is key because it dictates the choice of pharmacokinetic parameters that can be accurately extracted by T_1 -weighted MRI measurements of transcapillary and transcytolemmal exchange (24,25), as well as in contrast-agent based cellular imaging studies (26). Incorrect modeling of transcapillary water exchange results in, e.g., inaccurate extraction of tissue blood flow and volume estimates (8,27,28). The chemical exchange model has been compared (29) with classical Carr-Purcell diffusion theory, inner- and outer-sphere theory and the magnetised cylinder model (see Refs. 17 and 19, and references therein) for the case of weak dephasing.

This brief review suggests that the role of extravascular water diffusion in both susceptibility-induced NMR signal dephasing and compartmental relaxation is well understood theoretically. It appears, however, that the joint effect of (intracompartamental) diffusion and (intercompartmental) exchange of spins on the longitudinal magnetisation has, to date, not been addressed theoretically in the NMR literature, the well-mixed assumption being prevalent in most studies. In this work, we present a method that describes the spatio-temporal evolution of the longitudinal magnetisation in extravascular space and sets a mathematical framework for a more extensive treatment of tracer kinetics in future studies.

METHODS

Physical model

Tissue–blood exchange is mediated by water diffusion; this implies that magnetisation gradients are highest near the tissue–blood interface. Thus, tissues with a low capillary volume fraction (as is usually the case in physiologic tissues) can be subdivided into multiple capillary–tissue units, such that the total loss of magnetisation in the whole tissue is equal to the sum of the magnetisation losses in all such units. Following Krogh (30), a representative capillary–tissue unit is modeled as a long cylindrical region of radius A , embedding a coaxially placed capillary of radius a ; the radius of the pericapillary region is given by $A = a\zeta^{-1/2}$, where ζ is the capillary blood volume fraction. The capillary wall is modelled as a thin semipermeable membrane with diffusional water permeability κ . The extravascular region is assumed to be mesoscopically homogenous on the MRI timescale and, for present purposes, can be characterised by the apparent diffusivity of water, D_{ev} , and the longitudinal relaxation rate in the absence of exchange, R_{ev} (both assumed constant). The difference in the extravascular longitudinal magnetisation at equilibrium and at time t is denoted by $\psi_{ev}(\mathbf{r}, t)$; its spatio-temporal evolution is described by the Bloch-Torrey equation (6):

$$\frac{\partial \psi_{ev}}{\partial t} = [D_{ev} \nabla^2 - R_{ev}] \psi_{ev}, \quad (1)$$

and the flux conditions through the capillary wall and the pericapillary boundary:

$$D_{ev} \mathbf{n} \nabla \psi_{ev}|_{r=a} = \kappa [\psi_{ev} - \psi_{iv}]_{r=a}, \quad (2)$$

$$D_{ev} \mathbf{n} \nabla \psi_{ev}|_{r=A} = 0 \quad (3)$$

(\mathbf{n} is the unit outward normal). The zero-flux condition at the pericapillary boundary implies that a spin impinging on the outer boundary will be reflected back into the pericapillary region; that is, all spins in the diffusion watershed are affected equally, on average, by the surrounding capillary network, a reasonable modelling assumption.

In this study, we consider the limiting case of negligible blood magnetisation resulting from a high concentration of paramagnetic blood-pool tracer, i.e., $\psi_{iv} \ll \psi_{ev}$ in Eq. 2. This constitutes our chief technical assumption. The physical content of this limiting case is specified next. First, the mean residence time of water molecules in the well-mixed blood compartment is given by:

$$\tau_{iv} = \frac{V_{iv}}{\kappa S_{iv}} = \frac{a}{2\kappa}, \quad (4)$$

where S_{iv} is the capillary surface area and V_{iv} is the capillary volume. [Fast intracapillary mixing is largely the result of erythrocyte motion, ca. $1.5 \mu\text{m ms}^{-1}$ (31), rather than intracapillary water diffusion]. Further note that the product $R\tau_{iv}$, where $R = R_{iv} - R_{ev}$, gives the attenuation of the longitudinal magnetic moment of such molecules relative to the intravascular-to-extravascular exchange rate, τ_{iv}^{-1} ; hence, if

$$R\tau_{iv} \gg 1, \quad (5)$$

an intravascular spin becomes, on average, fully relaxed before it can (re)enter the pericapillary region. This physical reasoning is best illustrated by finding the density in the well-mixed intravascular compartment, $\psi_{iv}(t)$, that ensues on application of a spatially uniform, but otherwise arbitrary, extravascular density, $\psi_{ev}(t)$, with zero initial conditions. In the frequency domain, we have:

$$\psi_{iv}(\omega) = \frac{1}{-i\omega\tau_{iv} + 1 + R\tau_{iv}} \psi_{ev}(\omega). \quad (6)$$

Thus, the parameter $R\tau_{iv}$ does measure the smallness of $\psi_{iv}(t)$. In practice, however, if the blood Larmor frequency lies in the pass-band of the applied RF pulse, as is usually the case, then the condition $\psi_{iv} \ll \psi_{ev}$ may not hold strictly, at least at times $t \lesssim R^{-1}$. In the human brain, we estimated $R\tau_{iv} \sim 10-80$ for steady state ($\sim 3 \text{ mM}$) and peak ($\sim 18 \text{ mM}$) gadopentetate dimeglumine concentrations in blood (32) at 1.5 and 3 T; see Ref. 33 and Fig. 5.3 in Ref. 34 for tracer relaxivities and T_1 values, respectively. In human myocardium, we estimated $R\tau_{iv} \sim 0.5-5$ at 1.5 T for intravascular contrast agent (Feruglose) concentrations between 0.5–5 mg per body weight, see Ref. 10. For the above examples, the ratio of intravascular-to-extravascular magnetisation in brain tissue is low for a wide range of tracer concentrations, including first-pass and recirculation levels; in myocardium, this condition appears to be less well satisfied.

In the limiting case of negligible intravascular magnetisation, the constant relaxation rate R_{ev} enters into the

expression of $\psi_{\text{ev}}(\mathbf{r}, t)$ through the factor $\exp(-R_{\text{ev}}t)$, which is left understood in the sequel for simplicity. Further note that, in the case considered here, the effect of capillary blood flow on exchange becomes immaterial.

Physiologic Parameter Values

Literature values for relevant physiologic parameters are collected below for ease of reference.

a. *Human brain cortex*: capillary diameter, $2a = 6.5 \mu\text{m}$; mean intercapillary distance, $2A = 57 \mu\text{m}$; capillary blood volume fraction, $\zeta = 2.5\%$ (average values obtained from stereological data in Refs. 35 and 36); apparent diffusivity of water, $D = 0.8 \mu\text{m}^2 \text{ms}^{-1}$ (37); capillary permeability-surface area product for water in the central cortex, $PS = 1.5 \text{min}^{-1}$ (38); from this, the capillary water permeability is estimated as $\kappa = 1.6 \times 10^{-3} \mu\text{m} \text{ms}^{-1}$ from Eq. 16 below, consistent with Ref. 39.

b. *Myocardium*: average capillary diameter, $5.6 \mu\text{m}$; capillary segment lengths average $100 \mu\text{m}$, with a strongly right-skewed distribution (40) (figures for dog myocardium); intercapillary distance, $2A = 17.5\text{--}25 \mu\text{m}$ (5,18,40); $\zeta \approx 13\%$ in human myocardium (10); $D = 1\text{--}1.5 \mu\text{m}^2 \text{ms}^{-1}$, see Refs. 5, 18, 28 and references therein; and $\kappa = 3.8\text{--}5.2 \times 10^{-3} \mu\text{m} \text{ms}^{-1}$, see Applications section.

Definition of Effective Extravascular Depolarised Volume

The extravascular magnetisation, $\psi(\mathbf{r}, t)$, is a smooth function of both time and distance to the intravascular compartment, see Figs. 4 and 6 (the subscript ‘ev’ is dropped in the sequel where no confusion arises). The magnetisation gradient at the tissue–blood interface is proportional to the flux of magnetic moment into the blood compartment, see Eq. 2, which in turn results in decreased NMR signal, $S(t)$. Physically, the effective extravascular depolarised volume, $\Lambda(t)$, is proportional to the cumulative loss of extravascular magnetic moment, hence to signal reduction in the pericapillary region, as given by:

$$\frac{|S(t) - S(0)|}{S(0)} = \frac{\Lambda(t)}{V_{\text{ev}}}, \quad [7]$$

where V_{ev} is the extravascular volume. This relation motivates an operational definition of $\Lambda(t)$ in terms of the magnetisation density, $G(\mathbf{r}, \mathbf{r}', t)$, of a spin packet (i.e., a point source of magnetisation) placed at position \mathbf{r}' in the extravascular region at time $t = 0$. $G(\mathbf{r}, \mathbf{r}', t)$ is Green’s function (41) for Eqs. 1–3 in the extravascular region, and is also known as the diffusion propagator. The initial magnetisation can be normalised to unity because in most tissues the water proton density is nearly homogenous (5) and a uniform NMR excitation is assumed. Substitution of the NMR signal

$$S(t) \sim \int_{\text{ev}} \psi(\mathbf{r}, t) d^n \mathbf{r}, \quad [8]$$

where

$$\psi(\mathbf{r}, t) = \int_{\text{ev}} G(\mathbf{r}, \mathbf{r}', t) \psi(\mathbf{r}', 0) d^n \mathbf{r}', \quad [9]$$

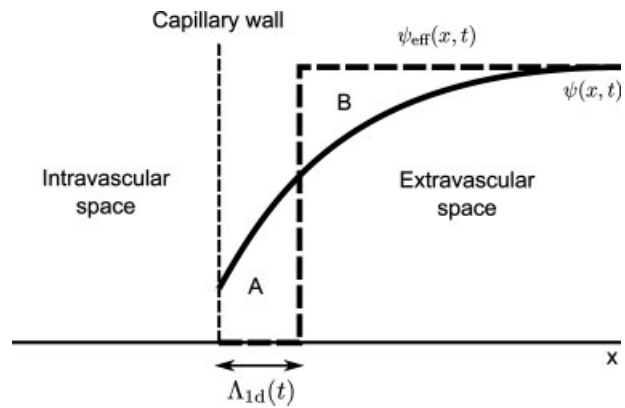


FIG. 1. Illustrating the definition of effective extravascular depolarised volume (one-dimensional case). Both the extravascular magnetisation $\psi(x, t)$ (solid line) and the effective magnetisation (dashed line) are shown schematically. The areas A and B are equal.

in Eq. 7, results in:

$$\Lambda(t) = \int_{\text{ev}} \left[1 - \int_{\text{ev}} G(\mathbf{r}, \mathbf{r}', t) d^n \mathbf{r}' \right] d^n \mathbf{r}, \quad [10]$$

where all integrals are taken over the extravascular region. A discussion of this result follows; detailed calculations of $\psi(\mathbf{r}, t)$ and $\Lambda(t)$ can be found in the Appendix.

Green’s function methods have been used in theoretical work on susceptibility-induced signal dephasing (16–19). The effective depolarised volume, as defined by Eq. 10, is analogous to a quantity introduced by Yablonskiy and Haacke (16) that represents the pericapillary volume in which signal dephasing is strongest (17). In Fig. 1, the ‘‘effective magnetisation’’, $\psi_{\text{eff}}(\mathbf{r}, t)$, is equal to $\psi(\mathbf{r}, 0) \equiv 1$ for $|\mathbf{r}| > \Lambda(t)$ and is zero elsewhere; hence, the total loss of extravascular magnetic moment to time t is numerically equal to the product $\psi(\mathbf{r}, 0) \cdot \Lambda(t)$. The inner integral in Eq. 10 gives the normalised magnetisation of a spin packet, $\Psi(\mathbf{r}', t)$, where $\Psi(\mathbf{r}', 0) = \int_{\text{ev}} G(\mathbf{r}, \mathbf{r}', 0) d^n \mathbf{r} = 1$ and $\Psi(\mathbf{r}', t > 0) \leq 1$; thus, the term in brackets gives the fraction of magnetisation lost in the extravascular region, and a further integration yields the volume where the extravascular NMR signal has become effectively depolarised by time t .

The plausibility of Eq. 10 is easily established for the two extreme permeability cases: (i) with an impervious capillary wall ($\kappa = 0$) the extravascular magnetic moment is conserved; hence, the integral of G is equal to unity for all t , which gives $\Lambda(t) = 0$, as expected; (ii) with a fully permeable capillary wall ($\kappa = \infty$), the extravascular magnetic moment decreases steadily over time; hence, at long times the integral of G vanishes and $\Lambda(t)$ approaches V_{ev} .

Using Eqs. 9, 10, the normalised, space-averaged extravascular magnetisation may be written in terms of $\Lambda(t)$ as:

$$\langle \psi(\mathbf{r}, t) \rangle = \frac{1}{V_{\text{ev}}} \int_{\text{ev}} \psi(\mathbf{r}, t) d^2 \mathbf{r} = 1 - \frac{\Lambda(t)}{V_{\text{ev}}}. \quad [11]$$

Summary of Monte Carlo Simulations

Computer simulations of tissue–blood exchange were performed using MATLAB programs written in-house. Extravascular diffusion was modelled by an ensemble of spin

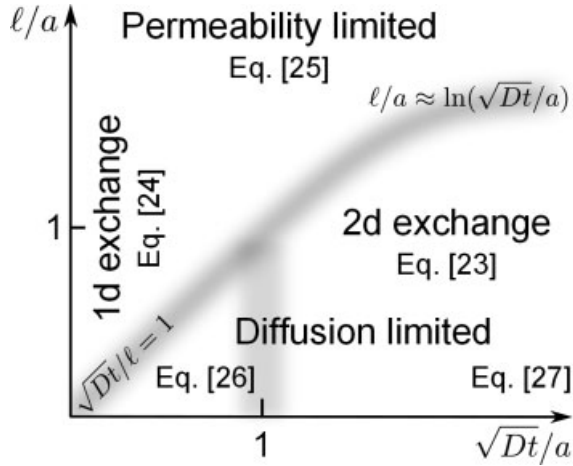


FIG. 2. Schematic diagram (arbitrary scale) of 2d exchange regimes for the case $a/A \ll 1$ in terms of the normalised diffusion length ($\zeta = \sqrt{Dt}/a$) and the effective membrane thickness normalised to capillary radius ($\ell/a = D/a\kappa$).

random walks consisting of independent, normally distributed steps with root mean squared length $\sigma = \sqrt{4D\Delta t}$, where Δt is the time step. Spins eventually traversed the capillary wall with permeability-dependent probability p , given by:

$$p = \min \left\{ 2\sqrt{\pi} \frac{\kappa \Delta t}{\sigma}, 1 \right\} = \min \left\{ \sqrt{\frac{\pi \Delta t}{\tau_\kappa}}, 1 \right\} \quad [12]$$

(τ_κ is defined in Eq. 15 below) whereupon they were removed from the ensemble, thus simulating full intracapillary relaxation. Equation 12 results by equating the flux of magnetic moment (for zero intravascular magnetisation and some constant, non-zero extravascular magnetisation) computed in two different ways: “macroscopically”, as per the definition of capillary permeability, Eq. 2, and “microscopically”, by means of the probability distribution associated to the random walk. It is assumed in Eq. 12 that $\sigma \ll a$ by allowing for a large number of diffusion steps. The size of the simulation box was chosen as a trade-off between the systematic error due to a finite box size, and the need to keep an adequate spin density throughout the simulation.

RESULTS

Extravascular Magnetisation and Effective Depolarised Volume

The extravascular magnetisation and the effective extravascular depolarised volume are given by Eqs. A7 and A8, respectively (see Appendix). These expressions simplify considerably for sparse capillary networks ($a/A \ll 1$), e.g., in brain and, to a lesser extent, myocardial tissue. The various tissue–blood exchange regimes are depicted schematically in Fig. 2. The two most important limiting cases, namely the permeability-limited regime and the diffusion-limited regime, are discussed at length in the sequel. As shown in Fig. 2, the following parameters enter into the expressions of $\psi(\mathbf{r}, t)$ and $\Lambda(t)$: first, the normalised

diffusion length,

$$\zeta = \frac{\sqrt{Dt}}{a}, \quad [13]$$

defines the timescale of exchange in sparse capillary networks; the effective membrane thickness,

$$\ell = \frac{D}{\kappa}, \quad [14]$$

is the width of a tissue slab across which the given concentration difference at the tissue–blood interface, $\Delta\psi|_{r=a}$, would ensue assuming steady flux conditions, see Eq. 2 and Fig. 3. Next, the normalised effective membrane thickness $\ell/a = D/a\kappa$ is the ratio of residence time to diffusion time for water molecules. (Note that this ratio is the same for both the intravascular and extravascular compartments, see Eqs. 4, 29). Lastly, the permeation time is defined as:

$$\tau_\kappa = \frac{\ell}{\kappa} = \frac{D}{\kappa^2}. \quad [15]$$

The ratio $\sqrt{t/\tau_\kappa}$ can be recast as (i) the ratio of flux per unit magnetisation difference ($= \kappa$) to two-dimensional (2d) diffusion rate ($= \sqrt{D/t}$); (ii) the ratio of “permeation length” ($= \kappa t$) to diffusion length ($\sim \sqrt{Dt}$); and (iii) the ratio of diffusion length to effective membrane thickness. The capillary permeability can be estimated from the measured capillary permeability-surface area product per volume of tissue if the mean capillary radius and capillary blood volume fraction are both known, thus:

$$PS = \frac{\kappa S_{iv}}{V_{iv} + V_{ev}} = \frac{2\kappa\zeta}{a} = \frac{\zeta}{\tau_{iv}}. \quad [16]$$

One-Dimensional Case

The situation in which $\psi(\mathbf{r}, t)$ changes appreciably only near the capillary wall is referred to in this work as the one-dimensional (1d) case, because then the capillary wall appears virtually flat to all the near-by diffusing spins (the capillary radius thus becomes immaterial); the 1d case is key in discussing two-dimensional (2d) exchange, as explained in the next subsection.

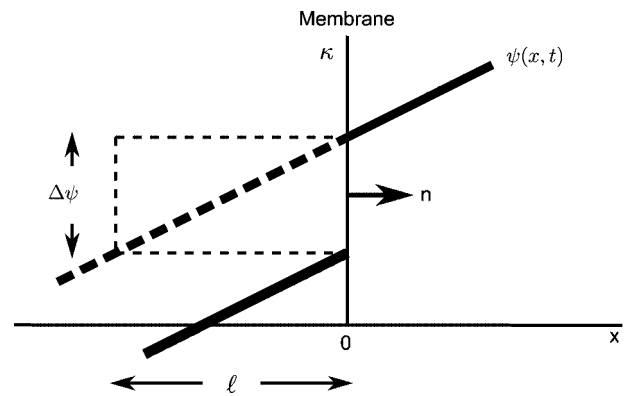


FIG. 3. Illustrating the effective membrane thickness, ℓ . The magnetisation profile $\psi(x, t)$ (thick solid line) creates a steady flux across the membrane. The dashed line shows the equivalent magnetisation profile entering into the definition of ℓ .

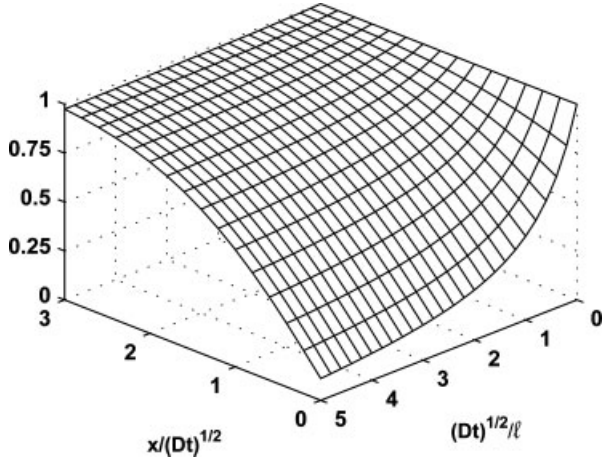


FIG. 4. 1d extravascular magnetisation for the case $a/A \ll 1$ as a function of both distance x from the capillary wall, normalised to diffusion length (x/\sqrt{Dt}), and diffusion length normalised to the effective membrane thickness (\sqrt{Dt}/ℓ).

For sparse capillary networks, the 1d extravascular magnetisation is given by (Fig. 4):

$$\psi_{1d}(x, t) = 1 - \operatorname{erfc}\left(\frac{x-a}{\sqrt{4Dt}}\right) + \exp\left(-\frac{(x-a)^2}{4Dt} + x'^2\right) \operatorname{erfc}(x'), \quad [17]$$

where $\operatorname{erfc}(\cdot)$ is the complementary error function and $x' = (x-a)/\sqrt{4Dt} + \sqrt{Dt}/\ell$. The magnetisation at the capillary wall at both short and long times becomes:

$$\psi_{1d}(a, t \rightarrow 0) \approx 1 - \frac{2}{\sqrt{\pi}} \frac{\sqrt{Dt}}{\ell}, \quad \psi_{1d}(a, t \rightarrow \infty) \approx \frac{1}{\sqrt{\pi}} \frac{\ell}{\sqrt{Dt}}, \quad [18]$$

respectively. As seen in Fig. 4, the timescale of exchange near the tissue–blood interface is set by the diffusion distance relative to the effective membrane thickness; for typical capillary water permeabilities in myocardium and brain (see Physiologic Parameter Values) the time point $\sqrt{Dt}/\ell = 5$ corresponds to an observation time of 2 to 12 min, respectively. Moreover, at distances greater than about three diffusion lengths, $\psi_{1d}(x, t)$ is hardly sensitive to the flux near the capillary wall. Thus, for tissue–blood exchange purposes, the sparsity condition for capillary networks is more precisely formulated as: $a, \sqrt{Dt} \ll A$.

The effective 1d extravascular depolarised volume is given by (Fig. 5):

$$\frac{\Lambda_{1d}(t)}{\ell} = \frac{2}{\sqrt{\pi}} \sqrt{\frac{t}{\tau_k}} + \exp\left(\frac{t}{\tau_k}\right) \operatorname{erfc}\left(\sqrt{\frac{t}{\tau_k}}\right) - 1. \quad [19]$$

It is easily checked that $\Lambda_{1d}(t)$ increases with κ and D , as expected on physical grounds.

In the permeability-limited regime, fast diffusive motion causes the flux of magnetic moment, hence also the extravascular magnetisation, to remain almost stationary near the tissue–blood interface; $\Lambda_{1d}(t)$ is thus expected

to be independent of D and to increase linearly with time. At short times, the rate of tissue–blood exchange is limited mainly by the capillary permeability, since only the spins in the region adjacent to the capillary wall have a non-negligible probability of traversing it. Based on the preceding physical arguments, we define the 1d permeability-limited regime by the condition $\sqrt{t/\tau_k} \ll 1$. In this regime,

$$\Lambda_{1d}(t) \approx \kappa t \Rightarrow \frac{\Lambda_{1d}(t)}{\ell} \approx \frac{t}{\tau_k}, \quad [20]$$

where the next leading term is of order $(t/\tau_k)^{3/2}$.

In the diffusion-limited regime, extravascular diffusion is a much slower process than capillary permeation; $\Lambda_{1d}(t)$ is thus expected to correlate with the diffusion length and to be largely independent of capillary permeability. Importantly, tissue–blood exchange at sufficiently long times is also limited by diffusive transport. Thus, the 1d diffusion-limited regime is defined by the condition $\sqrt{t/\tau_k} \gg 1$. In this regime,

$$\Lambda_{1d}(t) \approx \frac{2}{\sqrt{\pi}} \sqrt{Dt} - \ell \Rightarrow \frac{\Lambda_{1d}(t)}{\ell} \approx \frac{2}{\sqrt{\pi}} \sqrt{\frac{t}{\tau_k}} - 1, \quad [21]$$

the next leading term being of order $(t/\tau_k)^{-1/2}$.

Two-Dimensional Case

For sparse capillary networks, the 2d extravascular magnetisation is given by (Fig. 6):

$$\psi_{2d}(r, t) = \frac{2}{\pi} \int_0^\infty \frac{Y_0(q'r)P(q') - Q(q')J_0(q'r)}{[P^2 + Q^2](q')} \times \frac{\exp(-\zeta^2 q'^2)}{q'} dq', \quad [22]$$

where $r' = r/a$; ζ is defined by Eq. 13; $q' = aq$ is the normalised eigenfrequency; $J_0(\cdot)$, $Y_0(\cdot)$ are the Bessel functions

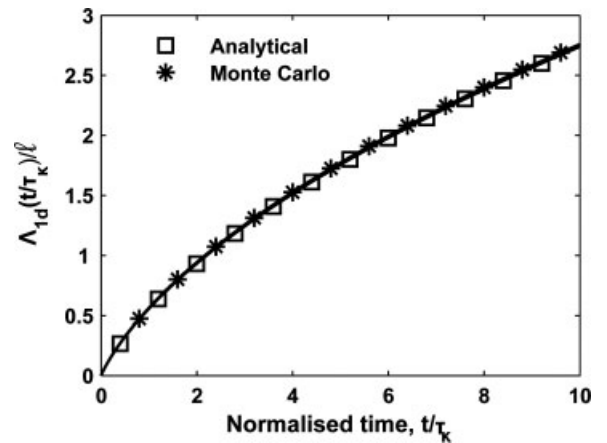


FIG. 5. Effective 1d depolarised volume normalised to effective membrane thickness ($\Lambda_{1d}(t)/\ell$) vs the normalised time ($\sqrt{t/\tau_k} = \sqrt{Dt}/\ell$): analytical expression (Eq. 19) and Monte Carlo simulation results.

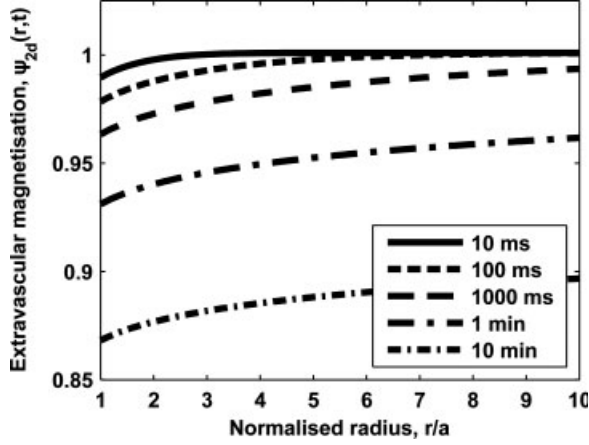


FIG. 6. 2d extravascular magnetisation vs normalised radius (r/a) for different values of the normalised diffusion length \sqrt{Dt}/a corresponding to the indicated observation times. Physiologic parameter values are representative of human myocardium, see Physiologic Parameter Values section; capillary water permeability, $\kappa = 5.2 \times 10^{-3} \mu\text{m ms}^{-1}$. Numerical integration introduces an excess error of about 0.2%.

of the first and second kind and order zero, respectively; and

$$P(q') = J_0(q') + (\ell/a)q'J_1(q'), \quad Q(q') = Y_0(q') + (\ell/a)q'Y_1(q').$$

The effective 2d extravascular depolarised volume is given by:

$$\Lambda_{2d}(t) = \frac{8a^2}{\pi} \int_0^\infty \frac{1 - \exp(-\zeta^2 q'^2)}{[P^2 + Q^2](q')} \frac{dq'}{q'^3}. \quad [23]$$

The quantities $\zeta = Dt/a^2$ and $\ell/a = D/a\kappa$ jointly characterize the various 2d exchange regimes, as discussed next (see Fig. 2).

If the diffusion length is small relative to the capillary radius ($\sqrt{Dt}/a \ll 1$), exchange is effectively confined to a thin pericapillary region next to the tissue–blood interface and thus appears one-dimensional, as discussed previously. The effective extravascular depolarised volume is then related to its 1d counterpart by:

$$\Lambda_{2d}(t) \approx 2\pi a \Lambda_{1d}(t). \quad [24]$$

In the permeability-limited regime, the condition $\sqrt{t}/\tau_\kappa \ll 1$ is equivalent to $\sqrt{Dt}/a \ll \ell/a$, hence substitution of Eq. 20 into Eq. 24 gives:

$$\Lambda_{2d}(t) \approx 2\pi a \kappa t \Rightarrow \frac{\Lambda_{2d}(t)}{A_{iv}} \approx \frac{PS}{\zeta} t = \frac{t}{\tau_{iv}} \quad [25]$$

with use of Eq. 4; A_{iv} is the capillary cross-sectional area. Note that $t/\tau_{iv} \ll 1$, by the conditions $\sqrt{Dt}/a \ll 1$ and $\sqrt{t}/\tau_\kappa \ll 1$. In the diffusion-limited regime, the condition $\sqrt{t}/\tau_\kappa \gg 1$ gives:

$$\Lambda_{2d}(t) \approx 4\pi^{1/2} a \sqrt{Dt} \Rightarrow \frac{\Lambda_{2d}(t)}{A_{iv}} \approx 4\pi^{-1/2} \frac{\sqrt{Dt}}{a}. \quad [26]$$

If the diffusion length is much greater than the capillary radius ($\sqrt{Dt}/a \gg 1$) the exchange becomes essentially two-dimensional and

$$\frac{\Lambda_{2d}(t)}{A_{iv}} \approx \frac{2Dt/a^2}{\ln(\sqrt{4Dt}/a) + \ell/a - \gamma}, \quad [27]$$

where $\gamma \approx 0.5772$ is Euler's constant. If $\ln(\sqrt{Dt}/a) \gg \ell/a$, tissue–blood exchange is limited by diffusive transport; if the reverse inequality holds, the exchange is limited by the capillary permeability and $\Lambda_{2d}(t)$ is again given by Eq. 25. Thus, in the permeability-limited regime, the formula $\Lambda_{2d}(t) \approx 2\pi a \kappa t$ remains valid even at long diffusion times.

Figure 7 shows excellent agreement between the analytical result, Eq. 23, and Monte Carlo simulations.

APPLICATIONS

Chemical Exchange Theory

If the diffusional motion of spins in the pericapillary region is sufficiently fast relative to capillary permeation, the extravascular magnetisation rapidly averages out, effectively varying only with the time. Then, integrating the Bloch-Torrey equation 1 over the pericapillary cross-section yields:

$$\frac{d\psi_{ev}(t)}{dt} = \frac{\psi_{iv}(t) - \psi_{ev}(t)}{\tau_{ev}} - R_{ev}\psi_{ev}(t), \quad [28]$$

where $\psi_{iv}(t)$, $\psi_{ev}(t)$ are space-averaged densities and the mean residence time of water molecules in the pericapillary region, τ_{ev} , is given by:

$$\tau_{ev}^{-1} = \frac{2\pi a \kappa}{A_{ev}} = \frac{PS}{1 - \zeta}. \quad [29]$$

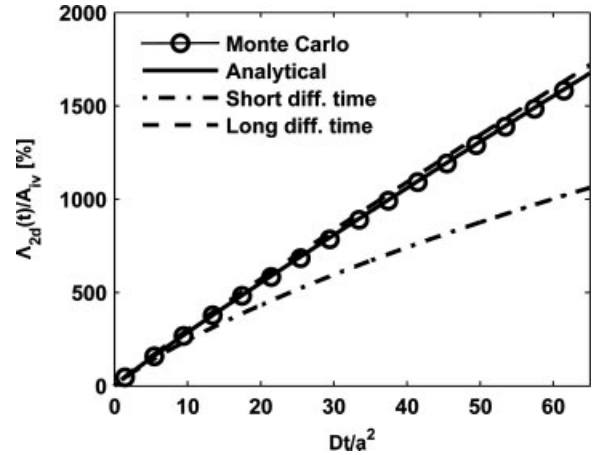


FIG. 7. Effective 2d depolarised volume normalised to the capillary cross section ($\Lambda_{2d}(t)/A_{iv}$) vs normalised squared diffusion length (Dt/a^2). Monte Carlo simulation results practically overlap with the analytical result, Eq. 23. The asymptotic bounds (dashed lines) at both short and long diffusion times are also shown. The curve labelled ‘analytical’ was obtained by numerical integration of Eq. 23; the long-time asymptote was obtained by piecewise analytical integration of Eq. 23, see Eqs. A25–A27; hence the slight discrepancy. Physical model parameters are: $a = 3.5 \mu\text{m}$, $D = 1.0 \mu\text{m}^2 \text{ms}^{-1}$ and $\kappa = 5.0 \times 10^{-2} \mu\text{m ms}^{-1}$.

The first term on the right-hand side of Eq. 28 follows from:

$$\begin{aligned} \frac{1}{A_{\text{ev}}} \int_{\text{ev}} D \nabla^2 \psi_{\text{ev}}(r, t) d^2 \mathbf{r} &= \frac{D}{A_{\text{ev}}} \left[2\pi r \frac{\partial \psi_{\text{ev}}(r, t)}{\partial r} \right]_a \\ &= \frac{2\pi a \kappa}{A_{\text{ev}}} [\psi_{\text{iv}}(a, t) - \psi_{\text{ev}}(a, t)] \\ &\approx \frac{\psi_{\text{iv}}(t) - \psi_{\text{ev}}(t)}{\tau_{\text{ev}}}, \end{aligned} \quad [30]$$

with use of the flux conditions, Eqs. 2, 3, and the fast diffusion approximation. Equation 28 is the basic equation of intravascular–extravascular chemical exchange for the longitudinal magnetisation. As expected, it expresses the balance of extravascular magnetic moment, including relaxation losses.

The condition $|R_{\text{iv}} - R_{\text{ev}}| \tau_{\text{iv}} \gg 1$, see Eq. 5, implies that the extravascular water undergoes slow transcapillary exchange (23). The effective extravascular relaxation rate is then approximately given by $R_{\text{ev}} + \tau_{\text{ev}}^{-1}$, where R_{ev} is the relaxation rate in the absence of exchange (23). This follows at once from Eq. 28 for the particular case considered in this work (i.e., $\psi_{\text{iv}} \ll \psi_{\text{ev}}$). Note, for comparison, that the increase in the longitudinal relaxation rate due to extravasation of a paramagnetic tracer depends, in addition, on the specifics of tracer compartmentalisation, concentration and relaxivity value; see, e.g., Ref. 28 for an experimental demonstration of the effect of transcapillary exchange on tissue T_1 in animal models using both intravascular and extracellular contrast agents.

The theory presented herein also reproduces the above result, as can be seen by rewriting the extravascular depolarised volume for the permeability-limited case, Eq. 25, in terms of τ_{ev} and substituting into the expression for the average density, Eq. 11. Thus,

$$\frac{\psi_{\text{ev}}(t)}{\psi_{\text{ev}}(0)} \approx \left(1 - \frac{t}{\tau_{\text{ev}}} \right) \exp(-R_{\text{ev}} t) \approx \exp\left(-\frac{t}{\tau_{\text{ev}}} - R_{\text{ev}} t \right). \quad [31]$$

The exponential approximation above is justified because $t/\tau_{\text{ev}} \sim a\kappa/D$ in the diffusional steady-state, where $a\kappa/D$ is typically much smaller than unity.

In conclusion, the Bloch-Torrey model reproduces the chemical exchange model of longitudinal magnetisation in the limiting case of fast intracompartamental diffusion.

Estimation of the Effective Extravascular Depolarised Volume by T_1 -based Methods

Donahue et al. (27,42) investigated the effect of transcapillary water exchange on the quantification of tissue blood volume using T_1 and T_1 -weighted MR measurements with intravascular tracers. By applying chemical exchange theory in NMR measurements in a rat model and in computer simulations of water exchange under various conditions, these investigators showed that tissue blood volume estimates are highly sensitive to exchange modelling assumptions. For slow transcapillary exchange (i.e., magnetic relaxation dominates over capillary permeation as per Eq. 5) and with a fully relaxed intravascular space (i.e., the main technical assumption of the present study),

the apparent capillary blood volume fraction, ζ_{app} , was found to be (27):

$$\zeta_{\text{app}} = \zeta \left(1 + \frac{T_1}{\tau} \right), \quad [32]$$

where T_1 is the pulse-sequence inversion time and

$$\tau^{-1} = \tau_{\text{iv}}^{-1} + \tau_{\text{ev}}^{-1} \quad [33]$$

is the net transcapillary water exchange rate (21). Equation 32 quantifies the effect of tissue–blood exchange on tissue blood volume estimates. For sparse capillary networks, $\tau^{-1} = \tau_{\text{iv}}^{-1}$ to first-order in $(a/A)^2$; hence, the relative error between the true and apparent capillary blood volume due to neglect of intracompartamental diffusion is given, approximately, by T_1/τ_{iv} , i.e., the normalised extravascular depolarised volume for the permeability-limited case, see Eq. 25. Under the above-stated conditions, this is the correction term provided by the model of tissue–blood exchange with account of extravascular diffusion.

Signal Attenuation Due to Tissue–Blood Exchange

In this subsection, we estimate the contribution of tissue–blood exchange to NMR signal attenuation (refer to Eq. 7) in brain and myocardium; unless otherwise noted, all parameter values are as given in the Physiologic Parameter Values subsection; an echo time of $T_E = 10$ ms for T_1 -weighted imaging is used for reference.

Brain: at short measurement times, the transcapillary exchange of magnetisation is strongly limited by the blood–brain barrier permeability; see Fig. 2 with $\ell/a \sim 10^2$ and $\sqrt{DT_E}/a \sim 1$. The effective depolarised volume thus becomes $\Lambda_{2d} \approx 2\pi a \kappa T_E$, from which $\Lambda_{2d}/A_{\text{iv}} \approx 1\%$.

Myocardium: Wacker et al. (10) estimated the transcapillary water exchange frequency (i.e., the permeability–surface area product, PS) and the capillary blood volume fraction, ζ , in patients with coronary artery disease. By fitting steady-state measurements of the longitudinal relaxation rate in blood and myocardium at 1.5 T (intravascular agent: Feruglose) to a model by Bauer et al. (8), these authors obtained $PS = 0.48 \text{ s}^{-1}$ and $\zeta = 12.9\%$. Assuming that it is the blood compartment that dominates the rate of transcapillary water exchange, Eq. 16 gives $\kappa = 5.2 \times 10^{-3} \mu\text{m ms}^{-1}$. In another study, Judd et al. (28) used a modified Krogh model of myocardial tissue consisting of intravascular, interstitial and intracellular spaces (volume fractions: 6.25%, 18.75% and 75%, respectively). The rate of transcapillary water exchange in the isolated, perfused rabbit heart was $\tau^{-1} = 2.7 \text{ s}^{-1}$ from steady-state, T_1 -weighted measurements at 4.7 T (intravascular agent: polylysine-gadopentetate dimeglumine). Equation 16 then gives $PS \approx \zeta \tau^{-1} = 0.17 \text{ s}^{-1}$ and $\kappa = 3.8 \times 10^{-3} \mu\text{m ms}^{-1}$ for myocardial water. These permeability estimates result in $\Lambda_{2d}/A_{\text{iv}} \approx 3\text{--}4\%$ in myocardium for an echo time of 10 ms.

Thus, the present model correctly predicts the well-known fact that capillary water permeability remains the main limiting factor in normal brain–blood exchange in the presence of paramagnetic blood-pool tracers; this conclusion also holds for myocardial water exchange. It can be concluded that, in the cases considered, the effect of tissue–blood exchange on the NMR signal is clearly

sub-dominant relative to the much stronger magnetic susceptibility effects.

DISCUSSION AND CONCLUSIONS

Model Accuracy

The validity of the capillary–tissue model described in Physical Model section relies on considerations concerning tissue morphometry and intercompartmental exchange. An *in vivo* study of the cat brain cortex (31) revealed a highly tortuous capillary network with significant interregional variability. Nevertheless, the values of the mean diameter, median radius of curvature, and median segment length for cortical capillaries (5.1, 57, and 108 μm , respectively) suggest that it is not unreasonable to model the individual capillaries, or segments of them, as long straight cylinders, each surrounded by a coaxial pericapillary region commensurate with the average capillary density. In fact, such a model closely resembles the arrangement of capillaries in striated muscle (30).

Further, it is crucial for the validity of the present model of tissue–blood exchange that the depolarised volumes associated with neighbouring capillaries do not overlap significantly. This is supported by a low capillary volume fraction in at least some tissues ($\zeta \sim 2.5\%$ and 10% in the brain and myocardium, respectively); only at capillary junctions do the depolarised volumes overlap somewhat, but the overall effect is negligible because the length of a capillary segment is, on average, much greater than the width of its associated depolarised region. In addition, having negligible overlap between adjacent depolarised regions relies on short observation times, such that $\sqrt{Dt} \ll A$; for example, $t \ll 100\text{--}1000$ ms for myocardium and brain tissue, respectively. Thus, for present purposes, if both the capillary radius and extravascular diffusion length are much smaller than the pericapillary radius, then the actual distribution of intercapillary distances becomes largely irrelevant (note that the pericapillary radius does not enter into any of the equations in the Results section) and the same holds true of the distribution of capillary orientations in sparse capillary networks.

The above discussion suggests that our results should remain valid even for complex three-dimensional capillary networks. A definite advantage of the Krogh capillary–tissue model is that it affords a tractable spatio-temporal description of the extravascular magnetisation for highly structured capillary beds (e.g., in myocardium). However, for highly irregular 3d capillary networks, such a detailed description is far less realistic; in this case, the space-averaged density and the effective extravascular depolarised volume for a representative capillary–tissue unit become the relevant quantities (these are mutually related through Eq. 11).

Concluding Remark

In this work we have theoretically evaluated tissue–blood exchange with account of extravascular diffusion in the limiting case of fast intravascular relaxation. First, we have calculated the time- and position-dependent longitudinal magnetisation in the extravascular region of a typical

Krogh capillary–tissue unit. Next, the effective extravascular depolarised volume has been obtained. This quantity is a direct measure of the NMR signal loss caused by tissue–blood exchange and can be experimentally determined by T_1 -based methods, at least in permeability-limited cases. The present method overcomes a potential limitation of chemical exchange models by accounting for intracompartmental diffusion.

The supporting mathematical framework (see the Appendix for details) can be extended to assess intravascular-to-extravascular flux of tracer, for example in arterial spin labeling and dynamic contrast-enhanced MR imaging methods. It can also be used to study diffusion of oxygen in a Krogh capillary–tissue unit (30,43,44).

APPENDIX: MATHEMATICAL FRAMEWORK

The extravascular magnetisation and the effective extravascular depolarised volume are calculated using a Green’s function approach (41) for the case $\psi_{iv} \ll \psi_{ev}$. Putting $\psi(\mathbf{r}, t) = f(\mathbf{r}) \exp(-\lambda t)$ in the Bloch-Torrey equation 1 yields the Sturm-Liouville eigenfunction equation:

$$[wf']' + wq^2f = 0, \quad [\text{A1}]$$

where $w = 1$ in the 1d case and $w = r$ in the 2d case, with the boundary conditions [2, 3]:

$$Df'|_{r=a} = \kappa f|_{r=a}, \quad Df'|_{r=A} = 0. \quad [\text{A2}]$$

The eigenvalues, λ_m , and spatial eigenfrequencies, q_m , are related by:

$$q_m^2 = \frac{\lambda_m - R_{ev}}{D}. \quad [\text{A3}]$$

Green’s function in the extravascular region is written as:

$$G(\mathbf{r}, \mathbf{r}', t) = \sum_{m=-\infty}^{\infty} \frac{f_m(\mathbf{r})f_m^*(\mathbf{r}')}{\|f_m\|^2} \exp(-\lambda_m t), \quad [\text{A4}]$$

where the 2d eigenfunction norm accounts for the cylindrical symmetry:

$$\|f_m\|^2 = \int_{ev} f_m^* f_m d^2\mathbf{r} = \int_0^{2\pi} d\phi \int_a^A f_m^* f_m r dr, \quad [\text{A5}]$$

where the asterisk denotes complex conjugation. Equation A4 satisfies the diffusion equation and the given boundary conditions, as well as the initial condition $G(\mathbf{r}, \mathbf{r}', 0) = \delta(\mathbf{r} - \mathbf{r}')$, whence:

$$\int_{ev} G(\mathbf{r}, \mathbf{r}', 0) d^2\mathbf{r} = 1. \quad [\text{A6}]$$

Termwise integration of $G(\mathbf{r}, \mathbf{r}', t)$ in the extravascular region, which is permissible by the uniform convergence (41,45), and substitution into Eq. 9 yields the extravascular magnetisation:

$$\psi(\mathbf{r}, t) = \frac{I_{cK}}{D} \sum_{m=-\infty}^{\infty} \frac{f_m^*|_{r=a} f_m(\mathbf{r}) \exp(-Dtq_m^2)}{\|f_m\|^2 q_m^2}, \quad [\text{A7}]$$

where $l_c = 2\pi a$. A further integration with account of the normalisation condition [A6] and substitution into Eq. 10 yields the effective extravascular depolarised volume:

$$\Lambda(t) = \left(\frac{l_c \kappa}{D}\right)^2 \sum_{m=0}^{\infty} \frac{|f_m|_{r=a}^2}{\|f_m\|^2} \frac{1 - \exp(-Dtq_m^2)}{q_m^4}. \quad [\text{A8}]$$

In the above equation, the f_m are real-valued eigenfunctions, hence the non-negative range of index m .

In arriving at Eqs. A7, A8, the following identity has been used:

$$\int_{\text{ev}} f_m(\mathbf{r}) d^2\mathbf{r} = \frac{l_c}{q_m^2} f'_m|_{r=a} = \frac{l_c \kappa}{Dq_m^2} f_m|_{r=a}. \quad [\text{A9}]$$

Equations A7, A8 must in general be handled numerically. They simplify considerably, however, for the case of sparse capillary networks ($a/A \ll 1$), as discussed in the next subsections.

One-Dimensional Case

In the 1d case, the wavelike eigenfunctions of Eq. A1 are given by:

$$f_m(x) = \exp(-iq_m x) - \exp(iq_m x + i2\delta_q) \quad [\text{A10}]$$

for $a \leq x \leq A$ and $m = 0, 1, 2, \dots$, where q_m is defined by Eq. A3 and δ_q is the so-called scattering phase. From the boundary condition at the capillary wall, Eq. 2, it follows that:

$$\delta_q = -aq_m + \tan^{-1} \ell q_m, \quad [\text{A11}]$$

where $\ell = D/\kappa$, see Eq. 14. The zero-flux condition at the pericapillary boundary yields the non-linear eigenfrequency relation:

$$Aq_m + \delta_q = (m + 1/2)\pi. \quad [\text{A12}]$$

Green's function can be written as:

$$G(x, x', t) = \sum_{m=0}^{\infty} \frac{\sin(q_m x + \delta_q) \sin(q_m x' + \delta_q)}{\|f_m\|^2} \exp(-Dtq_m^2), \quad [\text{A13}]$$

where the eigenfunction norm is:

$$\|f_m\|^2 = \frac{1}{2} \left[A - a + \frac{\ell}{1 + \ell^2 q_m^2} \right]. \quad [\text{A14}]$$

Integrating Eq. A13 yields $\Psi_{1d}(x, t)$, which becomes Eq. 17 for $a/A \ll 1$. Next, the extravascular depolarised volume follows from Eq. 10. Integrating $G(x, x', t)$ with use of Eqs. A11, A12 gives:

$$\int_a^A \int_a^A G(x, x', t) dx dx' = \sum_{m=0}^{\infty} \frac{1}{\|f_m\|^2} \frac{\exp(-Dtq_m^2)}{q_m^2(1 + \ell^2 q_m^2)}. \quad [\text{A15}]$$

The normalisation condition [A6] gives $V_{\text{ev}} = \int_a^A \int_a^A G(x, x', 0) dx dx'$, hence finally:

$$\Lambda_{1d}(t) = \sum_{m=0}^{\infty} \frac{1}{\|f_m\|^2} \frac{1 - \exp(-Dtq_m^2)}{q_m^2(1 + \ell^2 q_m^2)}. \quad [\text{A16}]$$

For sparse capillary networks, letting $A \rightarrow \infty$ in Eq. A16 with use of Eqs. A12, A14 results in:

$$\Lambda_{1d}(t) = \frac{2}{\pi} \int_0^{\infty} \frac{1 - \exp(-Dtq^2)}{1 + \ell^2 q^2} \frac{dq}{q^2}, \quad [\text{A17}]$$

which can be analytically integrated to yield Eq. 19.

Two-Dimensional Case

The eigenfunctions of Eq. A1 can be written (assuming cylindrical symmetry) as:

$$f_m(r) = \cos \delta_q J_0(rq_m) + \sin \delta_q Y_0(rq_m), \quad [\text{A18}]$$

for $0 < a \leq r \leq A$ and $0 \leq \phi < 2\pi$. The scattering phase δ_q results from the boundary condition at the capillary wall, Eq. 2, thus:

$$\tan \delta_q = -\frac{J_0(aq_m) + \ell q_m J_1(aq_m)}{Y_0(aq_m) + \ell q_m Y_1(aq_m)}. \quad [\text{A19}]$$

The zero-flux condition at the outer tissue boundary gives:

$$\cos \delta_q J_1(Aq_m) + \sin \delta_q Y_1(Aq_m) = 0. \quad [\text{A20}]$$

For sparse capillary networks, the large-argument asymptotic expressions for $J_1(\cdot)$ and $Y_1(\cdot)$ may be used, since A is then the highest-order infinite in the calculation. This results in:

$$Aq_m = (m + 1/4)\pi + \delta_q + O[A^{-1}]. \quad [\text{A21}]$$

Proceeding as in the 1d case, the extravascular magnetisation and the effective extravascular depolarised volume, Eqs. 22, 23, are obtained for the case of sparse capillary networks. These expressions cannot in general be analytically integrated for arbitrary values of ℓ/a and the time. The regimes of short and long diffusion times are both discussed in the next two subsections.

Two-Dimensional Exchange at Short Diffusion Times

The main result is: $\Lambda_{2d}(t) \approx 2\pi a \Lambda_{1d}(t)$, Eq. 24. A comparison between Eqs. 23 and A17 shows that the effective 2d depolarised volume can be recast as $\Lambda_{2d}(t) = 2\pi a[\Lambda_{1d}(t) + \epsilon(t)]$, where $\epsilon(t)$ can be neglected for sufficiently small t . The details of the proof suggest that the largest spectral content of $\Lambda_{2d}(t)$ lies in the eigenfrequency range: $\max\{1/a, \kappa/D\} < q < 1/\sqrt{Dt}$, with $\kappa \neq 0$. Moreover, it can be proved quite generally that $\Lambda_{2d}(t) \approx l_c \kappa t$ at short times, where l_c is the perimeter of the capillary cross section. The proof uses the definition of $\Lambda_{2d}(t)$, the diffusion equation and Green's theorem (41,45). From Eqs. 1, 9, 10:

$$-\frac{d\Lambda_{2d}(t)}{dt} = \int_{\text{ev}} \frac{\partial \Psi(\mathbf{r}, t)}{\partial t} d^2\mathbf{r} = \int_{\text{ev}} D\nabla^2 \Psi(\mathbf{r}, t) d^2\mathbf{r}, \quad [\text{A22}]$$

where $\Psi(\mathbf{r}, t) = \int_{\text{ev}} G(\mathbf{r}, \mathbf{r}', t) d\mathbf{r}'$ is the magnetisation of a spin packet. Use of Green's theorem and the boundary conditions [2, 3] gives:

$$\begin{aligned} \frac{d\Lambda_{2d}(t)}{dt} &= \oint_c D\mathbf{n} \nabla \Psi(\mathbf{r}, t) ds - \oint_{\text{ev}} D\mathbf{n} \nabla \Psi(\mathbf{r}, t) ds \\ &= \oint_c |\mathbf{j}|(a, t) ds = \kappa \oint_c \Psi(a, t) ds, \end{aligned} \quad [\text{A23}]$$

where \mathbf{n} is the unit outward normal. The above expression shows that $\Lambda(t)$ results from integration of the normalised magnetic moment lost to time t , as expected. At small t , $\Psi(a, t) = 1 + O[t^\alpha]$ (see for example Eq. 18), thus:

$$\frac{d\Lambda_{2d}(t)}{dt} = l_c \kappa + O[t^\alpha] \Rightarrow \Lambda_{2d}(t) = l_c \kappa t + O[t^{\alpha+1}]. \quad [\text{A24}]$$

Two-Dimensional Exchange at Long Diffusion Times

$\Lambda_{2d}(t)$ is estimated by piecewise integration of Eq. 23 with use of the appropriate asymptotic expressions for the Bessel functions and the $[1 - \exp(-\zeta^2 q^2)]q^{-3}$ term. First, for $0 \leq q < 1/\sqrt{Dt}$:

$$\Lambda_a(t) = 4Dt \cot^{-1} \left[\frac{2}{\pi} \left(\ln \frac{\sqrt{4Dt}}{a} + \frac{\ell}{a} - \gamma \right) \right]. \quad [\text{A25}]$$

If $\ln(\sqrt{Dt}/a) + \ell/a \gg 1$, the estimate $\cot^{-1} z = z^{-1} + O[z^{-3}]$ affords the simpler expression:

$$\Lambda_a(t) \approx \frac{2\pi Dt}{\ln(\sqrt{4Dt}/a) + \ell/a - \gamma}. \quad [\text{A26}]$$

Next, for $1/\sqrt{Dt} \leq q < 1/a$:

$$\Lambda_b(t) \approx \frac{\pi Dt}{[\ln(\sqrt{4Dt}/a) + \ell/a - \gamma]^2} + T_0 + T, \quad [\text{A27}]$$

where T collects terms of order $Dt[\ln(\sqrt{4Dt}/a)]^{-m}$ ($m \geq 3$) and T_0 decreases rapidly with ℓ/a . Lastly, $\Lambda_c(t) = 4a^2[1 - (\ell/a) \cot^{-1}(\ell/a)]$ for $1/a \leq q < \infty$. It is seen that the right-hand term in Eq. A25 is dominant for all ℓ/a . Thus, at long diffusion times the spectrum of $\Lambda_{2d}(t)$ lies mainly in the range of eigenfrequencies $0 < q \lesssim 1/\sqrt{Dt}$.

REFERENCES

- Donahue KM, Weisskoff RM, Burstein D. Water diffusion and exchange as they influence contrast enhancement. *J Mag Reson Imag* 1997;7:102–110.
- Gillis P, Koenig SH. Transverse relaxation of solvent protons induced by magnetized spheres: application to ferritin, erythrocytes, and magnetite. *Magn Reson Med* 1987;5:323–345.
- Koenig SH, Kellar KE. Theory of proton relaxation in solutions of magnetic nanoparticles, including the superparamagnetic size range. *Acad Radiol* 1996;(Suppl 2):S273–S276.
- Kellar KE, Henrichs PM, Spiller M, Koenig SH. Relaxation of solvent protons by solute Gd^{3+} -chelates revisited. *Magn Reson Med* 1997;37:730–735.
- Bauer WR, Schulten K. Theory of contrast agents in magnetic resonance imaging: coupling of spin relaxation and transport. *Magn Reson Med* 1992;26:16–39.
- Torrey HC. Bloch equations with diffusion terms. *Phys Rev* 1956;104:563–565.
- Nadler W, Schulten K. Generalized moment expansion for Brownian relaxation processes. *J Chem Phys* 1985;82:151–160.
- Bauer WR, Hiller KH, Roder F, Rommer E, Ertl G, Haase A. Magnetization exchange in capillaries by microcirculation affects diffusion-controlled spin-relaxation: a model which describes the effect of perfusion on relaxation enhancement by intravascular contrast agents. *Magn Reson Med* 1996;35:43–55.
- Bauer WR, Roder F, Hiller KH, Han H, Fröhlich S, Rommel E, Haase A, Ertl G. The effect of perfusion on T_1 after slice-selective spin inversion in the isolated cardioplegic heart: measurement of a lower bound of intracapillary-extravascular water proton exchange rate. *Magn Reson Med* 1997;38:917–923.
- Wacker CM, Wiesman F, Bock M, Jakob P, Sanstede JJW, Lehning A, Ertl G, Schad LR, Haase A, Bauer WR. Determination of regional blood volume and intra-extracapillary water exchange in human myocardium using Feruglose: first clinical results in patients with coronary artery disease. *Magn Reson Med* 2002;47:1013–1016.
- Waller C, Kahler E, Hiller KH, Hu K, Nahrendorf M, Voll S, Haase A, Ertl G, Bauer WR. Myocardial perfusion and intracapillary blood volume in rats at rest and with coronary dilatation: MR imaging in vivo with use of a spin-labeling technique. *Radiol* 2000;215:189–197.
- Waller C, Hiller KH, Kahler E, Hu K, Nahrendorf M, Voll S, Haase A, Ertl G, Bauer WR. Serial magnetic resonance imaging of microvascular remodeling in the infarcted rat heart. *Circulation* 2001;103:1564–1569.
- Kahler E, Waller C, Rommel E, Belle V, Hiller KH, Voll S, Bauer W, Haase A. Perfusion-corrected mapping of cardiac regional blood volume in rats in vivo. *Magn Reson Med* 1999;42:500–506.
- Kiselev VG. On the theoretical basis of perfusion measurements by dynamic susceptibility contrast MRI. *Magn Reson Med* 2001;46:1113–1122.
- Kjølby BF, Østergaard L, Kiselev VG. Theoretical model of intravascular paramagnetic tracers effect on tissue relaxation. *Magn Reson Med* 2006;56:187–197.
- Yablonskiy DA, Haacke EM. Theory of NMR signal behavior in magnetically inhomogeneous tissues: the static dephasing regime. *Magn Reson Med* 1994;32:749–763.
- Kiselev VG, Posse S. Analytical theory of susceptibility induced NMR signal dephasing in a cerebrovascular network. *Phys Rev Lett* 1998;81:5696–5699.
- Bauer WR, Nadler W, Bock M, Schad LR, Wacker C, Hartlep A, Ertl G. Theory of the BOLD effect in the capillary region: an analytical approach for the determination of T_2^* in the capillary myocardium. *Magn Reson Med* 1999;41:51–62.
- Kiselev VG, Posse S. Analytical model of susceptibility-induced MR signal dephasing: effect of diffusion in a microvascular network. *Magn Reson Med* 1999;41:499–509.
- McConnell HM. Reaction rates by nuclear magnetic resonance. *J Chem Phys* 1958;28:430–431.
- Allerhand A, Gutowsky H. Spin-echo NMR studies of chemical exchange. I. Some general aspects. *J Chem Phys* 1964;41:2115–2126.
- Leigh JS. Relaxation times in systems with chemical exchange: some exact solutions. *J Magn Reson* 1971;4:308–311.
- McLaughlin AC, Leigh JS. Relaxation times in systems with chemical exchange: approximate solutions for the nondilute case. *J Magn Reson Med* 1973;9:296–304.
- Li X, Rooney WD, Springer Jr CS. A unified magnetic resonance imaging pharmacokinetic theory: intravascular and extracellular reagents. *Magn Reson Med* 2005;54:1351–1359. Erratum in: *Magn Reson Med* 2006;55:1217.
- Yankelev TE, Rooney WD, Li X, Springer CS Jr. Variation of the relaxographic “shutter speed” for transcytolemmal water exchange affects the CR bolus-tracking curve shape. *Magn Reson Med* 2003;50:1151–1169.
- Strijkers GJ, Hak S, Kok MB, Springer Jr CS, Nicolay K. Three-compartment T_1 relaxation model for intracellular paramagnetic contrast agents. *Magn Reson Med* 2009;61:1049–1058.
- Donahue KM, Weisskoff RM, Chesler DA, Kwong K, Bogdanov AA, Mandeville JB, Rosen BR. Improving MR quantification of regional blood volume with intravascular T_1 contrast agents: accuracy, precision, and water exchange. *Magn Reson Med* 1996;36:858–867.
- Judd RM, Reeder SB, May-Newman K. Effects of water exchange on the measurement of myocardial perfusion using paramagnetic contrast agents. *Magn Reson Med* 1999;41:334–342.
- Brooks R, Moyny F, Gillis P. On T_2 -shortening by weakly magnetized particles: the chemical exchange model. *Magn Reson Med* 2001;45:1014–1020.
- Krogh A. The number and distribution of capillaries in muscles with calculation of the oxygen pressure head necessary for supplying the tissue. *J Physiol* 1919;52:409–415.
- Pawlak G, Rackl A, Bing RJ. Quantitative capillary topography and blood flows in the cerebral cortex of cats: an *in vivo* microscopic study. *Brain Res* 1981;208:35–58.
- Albert MS, Huang W, Lee JH, Patlak CS, Springer CS Jr. Susceptibility changes following bolus injections. *Magn Reson Med* 1993;29:700–708.
- Rohrer M, Bauer H, Mintorovitch J, Requardt M, Weinmann HJ. Comparison of magnetic properties of MRI contrast media solutions at different magnetic field strengths. *Invest Radiol* 2005;40:715–724.

34. Tofts PS, ed. Quantitative MRI of the brain. Measuring changes caused by disease. Chichester, England, John Wiley & Sons. 2004.
35. Hunziker O, Abdel'Al S, Schulz U. The aging human cerebral cortex: a stereological characterization of changes in the capillary net. *J Gerontol* 1979;34:345–350.
36. Meier-Ruge W, Hunziker O, Schulz U, Tobler HJ, Schweizer A. Stereological changes in the capillary network and nerve cells of the aging human brain. *Mech Ageing Devel* 1980;14:233–243.
37. Le Bihan D, Turner R, Patronas N. Diffusion MR imaging in normal brain and in brain tumor. In D Le Bihan, editor, Diffusion and perfusion. Magnetic resonance imaging: applications to functional MRI. Raven Press; New York 1995. pp 134–140.
38. Herscovitch P, Raichle M, Kilbourn M, Welch M. Positron emission tomographic measurement of cerebral blood flow and permeability–surface area product of water using [^{15}O]water and [^{11}C]butanol. *J Cereb Blood Flow Metab* 1987;7:527–542.
39. Neuder MS, Jenkins BG, Chesler DA, Moore JB, Lauffer RB, Rosen BR. Estimation of the permeability of the blood brain barrier to water in vivo under normal and perturbed conditions. *Proc ISMRM, Issue S2*, San Francisco, California, USA 1991. p 707.
40. Bassingthwaite JB, Yipintsoi T, Harvey RB. Microvasculature of the dog left ventricular myocardium. *Microvasc Res* 1974;7:229–249.
41. Courant R, Hilbert D. *Methoden der Mathematischen Physik*, 4. Auflage. Berlin: Springer Verlag; 1993.
42. Donahue KM, Burstein D, Manning WJ, Gray ML. Studies of Gd-DTPA relaxivity and proton exchange rates in tissue. *Magn Reson Med* 1994;32:66–76.
43. Krogh A. The rate of diffusion of gases through animal tissues, with some remarks on the coefficient of invasion. *J Physiol* 1919;52:391–408.
44. Hudetz AG, Halsey Jr JH, Horton CS, Conger KA, Reneau DD. Mathematical simulation of cerebral blood flow in focal ischemia. *Stroke* 1982;13:693–700.
45. Kaplan W. *Advanced calculus*, 5th ed. Addison-Wesley Publishing Company, Boston, 2003.